The Astrophysical Journal, 633:210–217, 2005 November 1

HIGH EXCITATION MOLECULAR GAS IN THE MAGELLANIC CLOUDS

Alberto D. Bolatto
Department of Astronomy and Radio Astronomy Laboratory, University of California at Berkeley, 601 Campbell Hall, Berkeley, CA 94720-3411; bolatto@astro.berkeley.edu

Frank P. Israel
Sterrewacht Leiden, Leiden University, P.O. Box 9513, NL-2300 RA Leiden, Netherlands; israel@strw.leidenuniv.nl

and

Christopher L. Martin
Department of Physics and Astronomy, Oberlin College, Wright Laboratory of Physics, 110 North Professor Street, Oberlin, OH 44074-1088; chris.martin@oberlin.edu
Received 2005 May 2; accepted 2005 June 22

ABSTRACT

We present the first survey of submillimeter ^{12}CO $J = 4 \rightarrow 3$ emission in the Magellanic Clouds. The survey is comprised of 15 $6' \times 6'$ maps obtained using the AST/RO telescope toward the molecular peaks of the Large and Small Magellanic Clouds. We have used these data to constrain the physical conditions in these objects, in particular, their molecular gas density and temperature. We find that there are significant amounts of warm molecular gas associated with most of these molecular peaks and that high molecular gas temperatures are pervasive throughout our sample. We discuss whether this may be due to the low metallicities and the associated dearth of gas coolants in the Clouds and conclude that the present sample is insufficient to assert this effect.

Subject headings: galaxies: ISM — ISM: molecules — Magellanic Clouds — submillimeter

1. INTRODUCTION

With their proximity, unextinguished lines of sight, and profuse star formation, the Magellanic Clouds are some of the best extragalactic objects in which to study the relationship between molecules and star formation. Because the interstellar medium (ISM) in the Magellanic Clouds is deficient in heavy elements and dust, molecular observations of these objects probe an interesting regime, perhaps more similar to the conditions in early protogalaxies rather than to those prevalent today in the Milky Way. Indeed, studies of active, metal-poor, nearby dwarf galaxies such as the Magellanic Clouds should offer insight into the processes at work in primeval sources.

What are the effects of low metallicities on the star-forming molecular ISM? We know that molecules are more difficult to form both in the gas phase (less O, C, and N) and on grain surfaces (fewer grains) and that they are easier to destroy (diminished dust shielding of the UV radiation) in low-metallicity environments. Thus, molecules other than H_2 are rarer in these sources, which in particular translates into a dearth of CO emission in the Magellanic Clouds and other dwarf irregular galaxies (e.g., Israel et al. 1986, 1995; Taylor et al. 1998; Leroy et al. 2005). Furthermore, because the far-infrared and submillimeter lines of the different forms of carbon and oxygen (C^+, C, O, and CO) dominate the cooling of the star-forming ISM (e.g., Le Bourlot et al. 1993; Wolfire et al. 1995), the lower abundances of these elements will make the cooling of the molecular gas less efficient. However, at the same time smaller dust-to-gas ratios will yield lower heating of the molecular gas, as photoelectric ejection of electrons from small dust grains is the chief mode by which starlight heats the gas phase of the ISM. If molecular gas temperatures were considerably affected by the metallicity of the ISM, we expect important consequences for star formation in such environments. In particular, if the Jeans criterion is relevant to star formation, the mass of collapsible clouds grows for decreasing metallicity as the Jeans mass increases $M_J \sim T^{3/2}$. Such a change could have important effects on the initial mass function of stars in these systems. To a first approximation, models suggest that lowering the metallicity causes a similar decrement in both heating (by diminishing the dust-to-gas ratio) and cooling (by diminishing the C and O abundances; Wolfire et al. 1995).

It is important to realize, however, that there are many possibilities likely to complicate this simple picture. For example, if the dust-to-gas ratio were to decrease faster than the metallicity (as suggested by Lisenfeld & Ferrara 1998), or if there were a lack of very small dust grains in the low-metallicity ISM (as suggested by the faintness of the polycyclic aromatic hydrocarbon emission observed toward some of these sources; e.g., Madden 2000), the heating processes may become less efficient, and the balance may be shifted toward lower temperatures. Furthermore, because it is also necessary to consider the metallicity threshold below which hitherto secondary heat sources (e.g., chemical heating) become important, the effects of metallicity on the heating and cooling balance of molecular clouds are very difficult to address from a purely theoretical approach.

Answering some of these questions observationally requires studying the physical conditions of the molecular gas in nearby low-metallicity sources. At distances of 55 and 63 kpc, the proximity of the Magellanic Clouds affords single-dish millimeter-wave observations excellent spatial resolution attainable in other galaxies only through the use of interferometers, which permits detailed studies of individual clouds instead of ensemble properties. In particular, the ability to spatially separate the emission from different regions makes the Magellanic Clouds ideal targets to study the excitation of the molecular gas and its relationship with star formation. Multitransition studies of CO and other molecules are very useful tools to determine the physical conditions of the H_2 (e.g., Johansson et al. 1998;

TABLE 1
AST/RO AND SEST CO OBSERVATIONS OF MAGELLANIC CLOUD H II REGIONS

SOURCE (1)	COORDINATES R.A. (B1950.0) (2)	COORDINATES Decl. (B1950.0) (3)	OBSERVED ^{12}CO INTEGRATED INTENSITIES (K km s^{-1}) (43″) ($J = 1 \rightarrow 0$) (4)	(109″) ($J = 1 \rightarrow 0$) (5)	(109″) $J = 4 \rightarrow 3$) (6)
			LMC		
N48	05 25 46.6	−66 17 36	3.7	...	6.6 ± 0.7
N55A	05 32 30.0	−66 29 21	17.4	4.9	2.5 ± 0.5
N79	04 52 09.5	−69 28 21	21.3	...	6.0 ± 0.7
N83A	04 54 17.0	−69 16 23	21.1	6.6	10.4 ± 1.4
N113	05 13 40.2	−69 25 37	23.4	...	9.7 ± 0.9
N159W	05 40 01.5	−69 47 02	57.0	45.6	20.8 ± 2.2
N167	05 44 17.6	−69 23 19	19.8	15.5	5.6 ± 1.1
N214C	05 42 21.8	−71 20 33	9.2	...	2.0 ± 0.4
LIRL 648	05 14 07.0	−69 38 57	13.1	...	6.7 ± 1.2
			SMC		
N12	00 44 50.5	−73 22 33	9.0	3.46	3.85 ± 0.7
N27	00 46 32.9	−73 21 50	11.6	5.63	5.0 ± 1.3
SMCB1#1	00 43 42.0	−73 35 10	4.1	2.67	≤ 0.5
SMCB2#6	00 46 28.1	−73 34 10	6.4	3.20	1.7 ± 0.9
N66	00 57 26.5	−72 26 36	0.9	3.41[a]	1.7 ± 1.1
N83	01 12 29.2	−73 32 40	5.6	2.66	2.0 ± 0.4

NOTES.—Nominal map center coordinates are indicated. Col. (5) contains the ^{12}CO $J = 1 \rightarrow 0$ integrated intensity in the $J = 4 \rightarrow 3$ beam for sources with $J = 1 \rightarrow 0$ maps. Units of right ascension are hours, minutes, and seconds, and units of declination are degrees, arcminutes, and arcseconds.

[a] Obtained from the ^{13}CO $J = 1 \rightarrow 0$ map convolved to a HPBW = 109″, assuming a ^{12}CO/^{13}CO ratio ≈11.

Heikkilä 1998; Chin et al. 1998; Heikkilä et al. 1999), but their application is limited if there is no information on the intensities of the higher CO transitions, which are extremely sensitive to density and temperature. Because of their southern declination, however, there is a dearth of submillimeter observations of the Clouds.

We present here a survey of ^{12}CO $J = 4 \rightarrow 3$ in the molecular peaks of the Magellanic Clouds and the results of an excitation analysis using these and lower J observations. These pointings were selected among the brightest ^{12}CO $J = 1 \rightarrow 0$ peaks found by Swedish-ESO Submillimeter Telescope (SEST) observations (Israel et al. 1993), many of which are associated with star-forming complexes and Henize (1956) Hα nebulosities and are thus denoted using the corresponding "N" number. In § 2 we present the observations, in § 3 we discuss the large velocity gradient (LVG) analysis and its results, and in § 4 we summarize our conclusions.

2. OBSERVATIONS AND RESULTS

We observed the $J = 4 \rightarrow 3$ transition of carbon monoxide (^{12}CO) at $\nu \simeq 461.0408$ GHz (650.7 μm) using the Antarctic Submillimeter Telescope and Remote Observatory (AST/RO), located at the Amundsen-Scott South Pole base (Stark et al. 2001). The observations were obtained on the austral winter of 2002, using the lower frequency side of the dual AST/RO superconductor-insulator-superconductor waveguide receiver (Walker et al. 1992; Honingh et al. 1992), with system temperatures of $T_{\rm sys} \sim 2000$ K. The back end was the 2048 channel low-resolution (1.07 MHz resolution, 0.68 MHz channels) acousto-optical spectrometer (Schieder et al. 1989). The spectra were observed in position-switching mode, chopping 25′ in azimuth (which is the same as right ascension at the pole). At 461 GHz, the telescope beam was measured to have a HPBW ≈ 109″. The forward efficiency determined from skydips was ∼70% and is assumed to be identical to $\eta_{\rm mb}$. Maps of size 6′ × 6′ centered on the SEST coordinates (see Table 1) were obtained for each region, using a 30″ grid. (In a few cases the maps were done on a 60″ grid.) The data were calibrated using the standard procedure for AST/RO, which includes sky, ambient, and cold-load measurements every 20–30 minutes, and processed using the COMB astronomical package. The individual maps are shown in Figure 1, and representative spectra are shown in Figures 2 and 3. Because the pointing accuracy is estimated to be ∼1′, we have selected the emission peaks closest to the center of the map within those margins to measure the integrated intensities compiled in Table 1 (indicated by crosses in Fig. 1). Note that this method may introduce a bias in the direction of obtaining larger CO $J = 4 \rightarrow 3$/CO $J = 1 \rightarrow 0$ ratios. Nonetheless, we feel that this methodology is justified, as in the Milky Way the positional coincidence between the peaks of both transitions is very often observed. In some cases it is apparent that the structure of the sources is complex (e.g., N159W; Bolatto et al. 2000), and in particular for N167 and N83 the brightest emission peak is well away from the central position. Given the large and variable effects of the atmosphere at submillimeter wavelengths and the pointing accuracy of the telescope, we estimate the overall absolute calibration accuracy of the data to be ∼30%.

Table 1 summarizes our observations. Column (4) lists the ^{12}CO $J = 1 \rightarrow 0$ integrated intensities observed by the SEST Magellanic Cloud Key Programme toward our sources, while column (5) shows the intensities convolved to the angular resolution of AST/RO. Finally, column (6) lists the ^{12}CO $J = 4 \rightarrow 3$ integrated intensities used in our LVG analysis, with

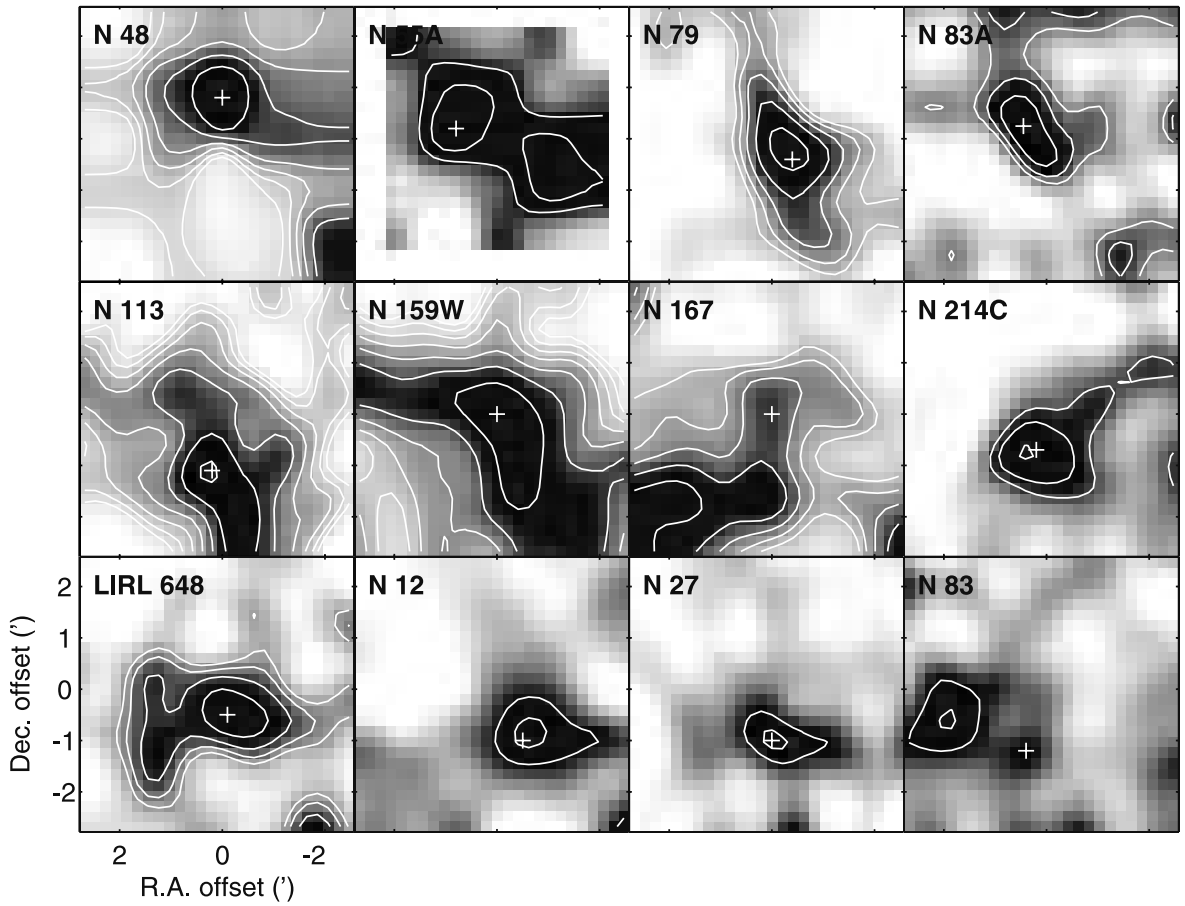

FIG. 1.—Plot of ^{12}CO $J = 4 \rightarrow 3$ maps obtained toward our detected sources in the LMC/SMC. The coordinates of the central positions of the maps [offsets (0, 0)] are listed in Table 1. The contours are logarithmically spaced, starting at 1.5 K km s^{-1} and increasing by factors of 1.3 (except for N79, N83A, N113, and N159W, where they start at 2.5 K km s^{-1}). These maps were produced by convolving the data with a Gaussian of FWHM $= 1'$. Most maps are sampled on a $30''$ grid, except for N48 and N55A, where the grid spacing used was $60''$. The positions marked by the crosses are those of the CO $J = 1 \rightarrow 0$ sources, where we measured the intensities used in the LVG analysis.

their statistical errors. These intensities are those measured in the AST/RO pointings marked with crosses in Figure 1.

3. ANALYSIS AND DISCUSSION

3.1. *Modeling of* CO

The available observed ^{12}CO and ^{13}CO line ratios have been modeled using the LVG radiative transfer models described by Jansen (1995) and Jansen et al. (1994). These models provide line intensities as a function of three input parameters: gas kinetic temperature T_k, molecular hydrogen density $n(\mathrm{H_2})$, and CO column density per unit velocity [$N(\mathrm{CO})/dV$]. By comparing model line *ratios* to the observed ratios we determine the physical parameters best describing the conditions in the observed source. In principle, with two isotopes we need to measure five independent line intensities in order to fully determine the conditions of a single molecular gas component [i.e., T_k, $n(\mathrm{H_2})$, $N(^{12}\mathrm{CO})/dV$, $N(^{13}\mathrm{CO})/dV$, and a beam filling factor]. By assuming a fixed isotopic abundance $[^{12}\mathrm{CO}]/[^{13}\mathrm{CO}] = 40$ (Johansson et al. 1994), we may decrease this requirement to four independent line intensities. As Table 2 shows, this minimum requirement is met by two out of nine Large Magellanic Cloud (LMC) objects and five out of six Small Magellanic Cloud (SMC) objects. The physical conditions of the remaining eight objects are, in principle, underdetermined.

More realistic, and consequently more complex, models of gas excitation that include more than one component require many more observations to be properly constrained. Full modeling of a two-component molecular cloud using two isotopes requires 10 independent measurements, which again are reduced to eight by the introduction of a fixed isotopic abundance. As this is more than we have actually observed in any of the LMC or SMC clouds, it is clear that the solutions may not be unique. As long as the range of possible solutions is not excessive, however, they are still useful to constrain the physical parameters governing the observed emission.

We identified acceptable fits by searching a grid of model parameter combinations [$10\ \mathrm{K} \leq T_k \leq 150\ \mathrm{K}$, $10^2\ \mathrm{cm^{-3}} \leq n(\mathrm{H_2}) \leq 10^5\ \mathrm{cm^{-3}}$, $6\times10^{15}\ \mathrm{cm^{-2}}\ (\mathrm{km\ s^{-1}})^{-1} \leq N(\mathrm{CO})/dV \leq 3\times 10^{18}\ \mathrm{cm^{-2}}\ (\mathrm{km\ s^{-1}})^{-1}$] for model line ratios matching the observed values. Although errors in the line ratios increase the range of possible solutions, these ratios tend to define reasonably well-constrained regions of parameter space. The solutions are somewhat degenerate, as variations in the parameters may compensate one another. For instance, a simultaneous increase in kinetic temperature and decrease in $\mathrm{H_2}$ densities (or vice versa) yields similar line ratios (see § 3.2.3).

3.2. *Single-Component Fits*

3.2.1. *Objects with Two Measured Intensities*

For three objects (LMC-N48, LMC-N214C, and SMCB2#6) we only have intensities in the $J = 1 \rightarrow 0$ and $J = 4 \rightarrow 3$ transitions of ^{12}CO. The parameters of these clouds are thus

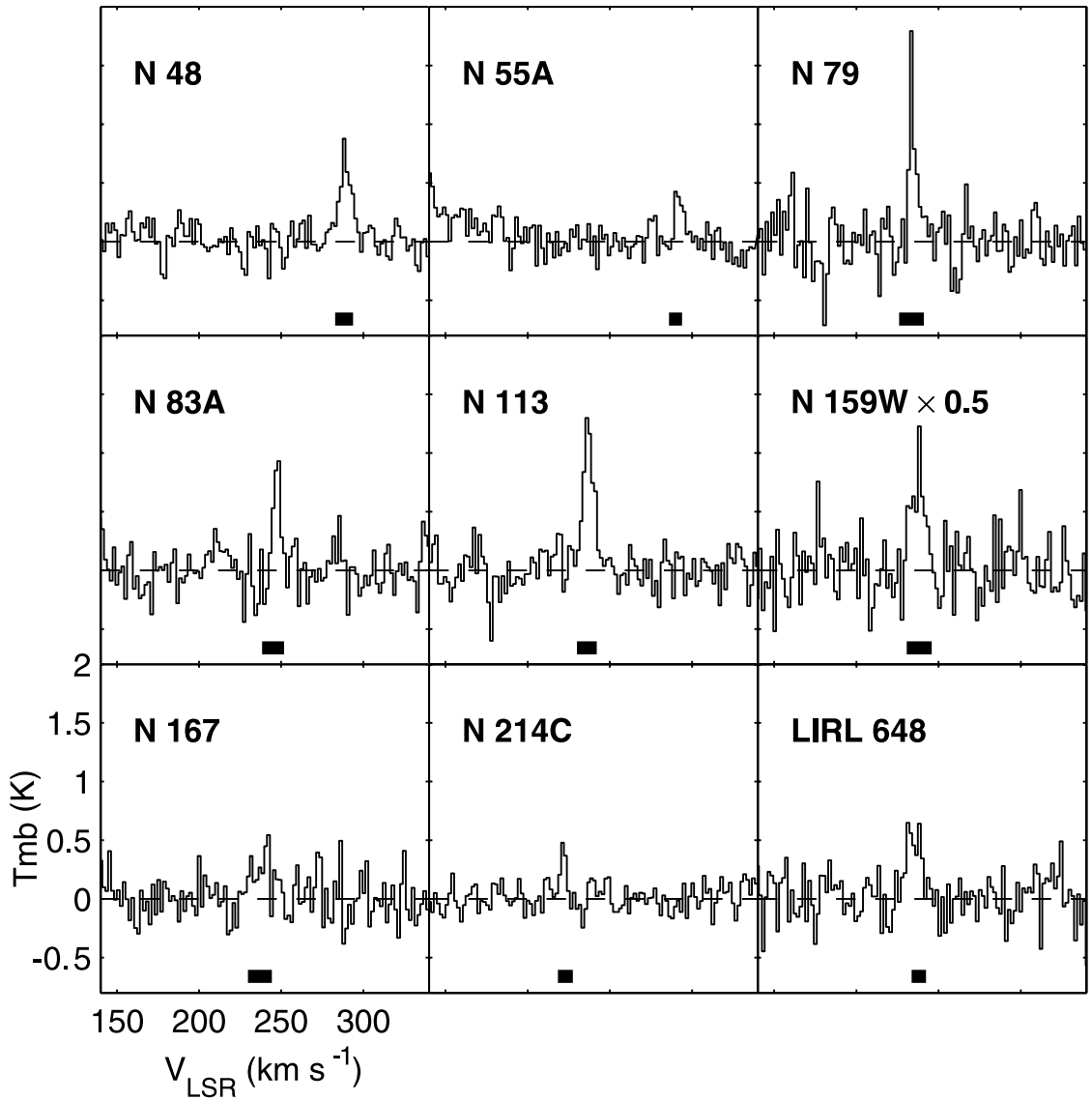

FIG. 2.—Spectra of ^{12}CO $J = 4 \rightarrow 3$ emission in LMC sources. These spectra were obtained toward the positions marked by crosses in Fig. 1. All sources were detected. The emission in N159W is shown scaled down by a factor of 2 for display purposes. The thick black line near the bottom of the plots indicates the velocity and width of the CO emission in the lower J transitions, as observed using SEST.

poorly constrained and not summarized in a table. Assuming a single molecular gas component, we find for SMCB2#6 no effective constraints: $T_k = 20$–150 K, $n(\mathrm{H_2}) = 10^2$–10^4 cm^{-3}, and $N(\mathrm{CO})/dV = 10^{16}$–$10^{18}$ cm^{-2}(km s^{-1})$^{-1}$. All ^{12}CO transitions should be very optically thick. LMC-N214C is slightly better determined: temperatures below 30 K are not allowed and densities appear high, $n(\mathrm{H_2}) = 10^4$–10^5 cm^{-3}. The $J = 1 \rightarrow 0$ transition should not be very optically thick (although the higher transitions are), and its isotopic intensity ratio should be 10–20, as is in fact commonly observed in the LMC (Israel et al. 2003). Finally, the high ^{12}CO $J = 4 \rightarrow 3$/CO $J = 1 \rightarrow 0$ ratio exhibited by LMC-N48 is, in the single-component approximation, only consistent with low optical depths (isotopic intensity ratios 20–40), rather high densities $n(\mathrm{H_2}) = 10^4$–10^5 cm^{-3} and temperatures $T_k = 60$–150 K, and gradients $N(\mathrm{CO})/dV = 10^{16}$–$10^{17}$ cm^{-2} (km s^{-1})$^{-1}$.

3.2.2. *Objects with Three Measured Intensities*

For five objects, all in the LMC (N55, N79, N83A, N113, and LIRL 648), we have measured ^{13}CO $J = 1 \rightarrow 0$ intensities in addition to the ^{12}CO $J = 1 \rightarrow 0$ and $J = 4 \rightarrow 3$ intensities. As is clear from the previous discussion, the molecular gas parameters are still underdetermined, but not fully unconstrained (Table 3). Both N79 and N113 fit very well to a hot and fairly dense model cloud with $T_k = 100$–150 K, $n(\mathrm{H_2}) = 3000$–5000 cm^{-3}, and a gradient of about 6×10^{17} cm^{-2} (km s^{-1})$^{-1}$. LIRL 648 is fitted, but not very well, by a gas at the somewhat lower temperature of 60 K and the somewhat higher density of 10^4 cm^{-3}. The physical parameters of the molecular gas cloud associated with N83A are inconsistent with the assumption of a single component. Only a very poor fit is obtained in the high-temperature, high-density, and high-velocity gradient limit.

3.2.3. *Objects with Four or More Measured Intensities*

Seven objects have a sufficiently large number of measured line intensities to allow a full determination of physical parameters, assuming they can be properly described by a single molecular gas component. This appears indeed to be the case for SMCB1#1, where we find excellent agreement between the observed ratios and those of a model gas characterized by

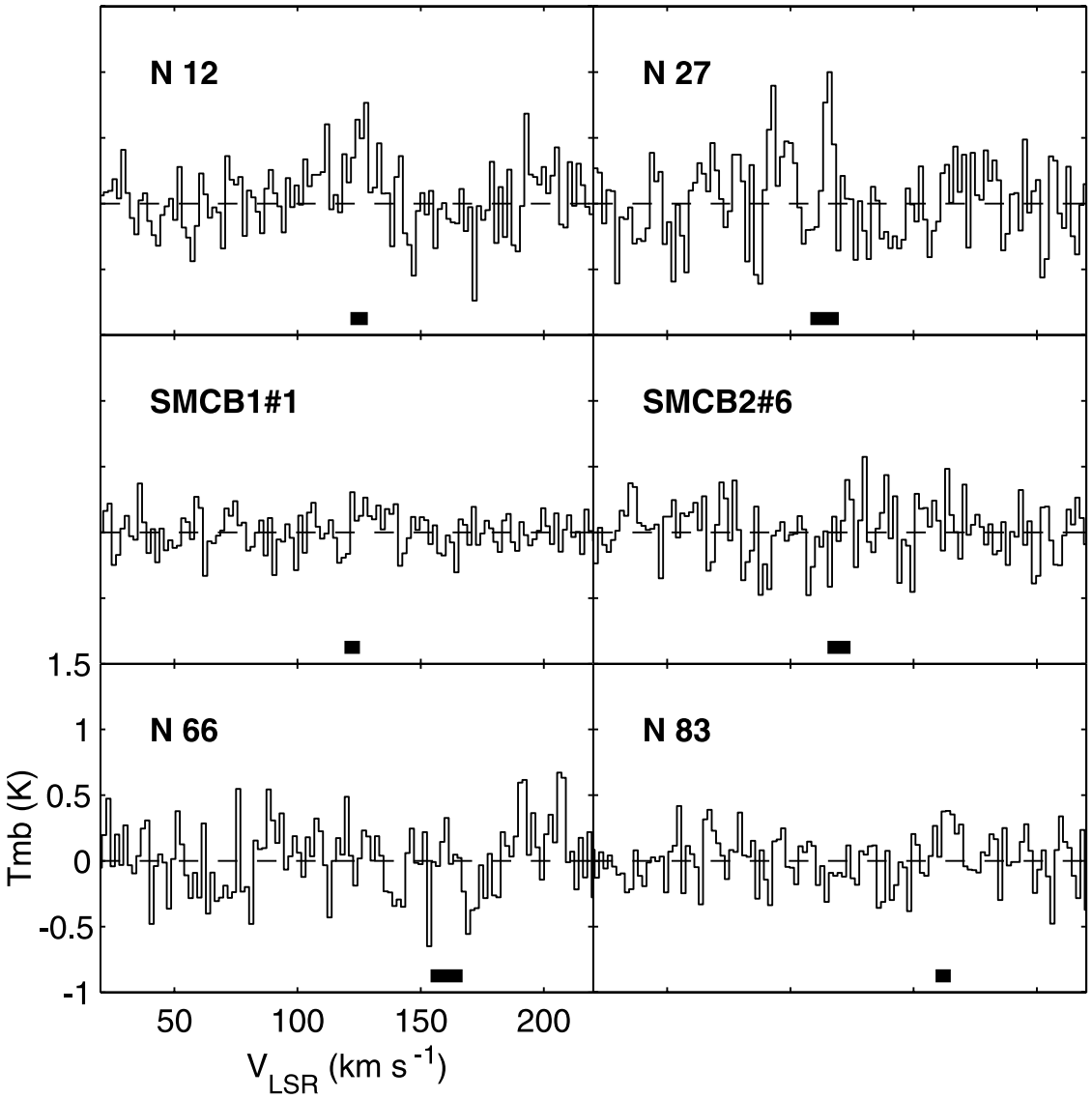

FIG. 3.—Spectra of ^{12}CO $J = 4 \rightarrow 3$ emission in SMC sources, obtained toward the positions marked with crosses in Fig. 1. Only N12, N27, and N83 were detected, and the signals are in general considerably weaker than in the LMC. As in the previous figure, the CO $J = 1 \rightarrow 0$ velocity and line width are indicated by the thick black line at the bottom of the plots.

TABLE 2

CO LINE INTENSITY RATIOS OF MAGELLANIC CLOUD OBJECTS

SOURCE	^{12}CO TRANSITION RATIOS			^{12}CO/^{13}CO ISOTOPIC RATIOS		REFERENCES
	(2 → 1/1 → 0)	(3 → 2/1 → 0)	(4 → 3/1 → 0)	(1 → 0)	(2 → 1)	
LMC						
N55A	...	...	0.51 ± 0.17	11	...	1, 2
N83A	...	...	1.58 ± 0.52	9	...	1, 3
N159W	0.90 ± 0.25	0.9	0.46 ± 0.15	9	5	1, 4, 5
N167	1.16 ± 0.23	...	0.36 ± 0.12	12	...	1, 6
SMC						
N12	1.20 ± 0.40	1.0	1.11 ± 0.28	11	9	1, 7
N27	0.95 ± 0.35	0.75	0.89 ± 0.30	17	11	1, 8, 9
SMCB1#1	0.72 ± 0.12	0.4	≤0.2	11	13.5	1, 10, 11
SMCB2#6	...	...	0.53 ± 0.28	...	...	1
N66	1.30 ± 0.35	1.0	0.50 ± 0.32	11	7	1, 9, 10
N83	1.19 ± 0.31	...	0.56 ± 0.22	10	9.5	1, 12

NOTE.—Ratios are determined from values in Table 1, and from previously published papers, mostly in the ESO Key Programme.

REFERENCES.—(1) This paper; (2) Israel et al. 1993; (3) Israel et al. 2003; (4) Johansson et al. 1998; (5) Bolatto et al. 2000; (6) Garay et al. 2002; (7) Chin et al. 1998; (8) Heikkilä et al. 1999; (9) Rubio et al. 1996; (10) Heikkilä 1998; (11) Rubio et al. 1993; (12) Bolatto et al. 2003.

TABLE 3
MODEL PHYSICAL PARAMETERS: SINGLE-COMPONENT FITS

Source	Kinetic Temperature T_k (K)	Volume Density $n(H_2)$ (cm^{-3})	Column Density $N(CO)/dV$ (cm^{-2} km^{-1} s)
		LMC	
N55	30–60	3×10^3	1×10^{17}
N79	100	5×10^3	$(6–10) \times 10^{17}$
N113	150	3×10^3	6×10^{17}
N159W	150	10^3	3×10^{17}
LIRL 648	60	10^4	3×10^{17}
		SMC	
SMCB1#1	50	7×10^2	0.5×10^{17}

$T_k = 50$ K, $n(H_2) = 700$ cm^{-3}, and $N(CO)/dV = 5 \times 10^{16}$ cm^{-2} $(km\ s^{-1})^{-1}$. To fine-tune the solutions, as well as to gain insight into the various trade-offs, we have run a finer grid of models for this particular source. We summarize the best solutions for the temperature range $T_k = 30–60$ K in Table 4. The overall best fit is achieved using a kinetic temperature $T_k = 50$ K and a density $n(H_2) = 700$ cm^{-3}. At constant temperature, the uncertainty in density is about 20%. From the table, it is also clear that we may allow for a similar temperature uncertainty of 20% if we simultaneously increase or decrease the density by 40%.

The good fit between model and observed line ratios is of particular significance because the solution is overdetermined with six independent intensity measurements. SMCB1#1 is a small and isolated molecular cloud in the SMC Bar, not associated with a star-forming region (Rubio et al. 1993, 2004; Reach et al. 2000); thus, a low density of $\sim$700 cm^{-3} is not necessarily surprising, although the kinetic temperature is higher than we would have expected for such a cloud in the Milky Way. Table 4, however, illustrates the difficulty in pinning down the physical conditions even in a simple cloud with a simple model.

The measured intensities of N159-W can also be fitted, albeit somewhat poorly, by a single hot ($T_k = 150$ K) and moderately dense component [$n(H_2) = 1000$ cm^{-3}]. However, none of the other five objects have intensities consistent with a single component. Typically, a component fitting the observed ^{12}CO line ratios would fail completely to explain the $^{12}CO/^{13}CO$ isotopic ratios, indicating that in addition to a warm gas component the presence of a second cooler and dense component should be assumed. The lack of associated luminous objects probably explains the exceptionally homogeneous nature of SMCB1#1, which is required for such a well-determined single-component fit to be valid.

3.3. *Dual-Component Fits*

Since (with the exception of SMCB1#1 and perhaps N159-W) *none* of the sources for which many constraints are available allows a good fit with a single gas component, we suspect that the successful single-component fits of the sources in Table 3 result primarily from insufficient information rather than from a simple physical structure. Attempts at more sophisticated modeling achieve little of value for most of these sources. The single exception is LMC-N83A, where only two observed ratios nevertheless conflict with every single-component model tried. A dual-component model yields acceptable but, not surprisingly, poorly constrained solutions (see Table 5). For all the other well-observed sources where single-component model fits failed, we have also constructed dual-component fits that are likewise listed in Table 5. This table shows that usually one of the two components component is reasonably well determined,

TABLE 4
MODEL FITS FOR SMCB1#1

T_{kin} (K)	$n(H_2)$ (cm^{-3})	$N(CO)/dV$ [$cm^{-2}(km\ s^{-1})^{-1}$]	$I^{12}CO/I^{13}CO$		^{12}CO ROTATIONAL RATIO		
			($J = 1 \rightarrow 0$)	($J = 2 \rightarrow 1$)	(1–0/2–1)	(3–2/2–1)	(4–3/2–1)
			Observed Constraints				
	...	...	11.2	13.5	1.4	0.6	$\leq$0.24
			Modeling Results				
60	500	6×10^{16}	10.4	12.0	1.41	0.56	0.23
50	600	5×10^{16}	11.4	12.2	1.45	0.54	0.21
50	700	5×10^{16}	12.0	12.2	1.43	0.56	0.23
50	800	5×10^{16}	12.4	11.8	1.40	0.57	0.24
40	1100	5×10^{16}	12.4	11.2	1.37	0.58	0.24
30	2000	4×10^{16}	14.1	10.8	1.30	0.59	0.24

TABLE 5
MODEL PHYSICAL PARAMETERS: DUAL-COMPONENT FITS

	"COLD DENSE" COMPONENT			"HOT TENUOUS" COMPONENT			
SOURCE	Kinetic Temperature T_k (K)	Volume Density $n(H_2)$ (cm^{-3})	Column Density $N(CO)/dV$ (cm^{-2} km^{-1} s)	Kinetic Temperature T_k (K)	Volume Density $n(H_2)$ (cm^{-3})	Column Density $N(CO)/dV$ (cm^{-2} km^{-1} s)	RELATIVE $J = 2-1$ ^{12}CO EMISSION
			LMC				
N83A.....	10	10^5	10×10^{17}	100	10^5	3×10^{17}	3 : 2
	60	10^5	1×10^{17}	150	$(5–10) \times 10^2$	$(6–10) \times 10^{17}$	4 : 1
	150	10^5	3×10^{17}	150	10^2	$(6–10) \times 10^{17}$	2 : 3
N159W.....	20	10^5	1×10^{17}	100	10^2	1×10^{17}	1 : 1
N167.....	20	10^4	0.6×10^{17}	30–60	$(1–10) \times 10^2$	$(0.3–10) \times 10^{17}$	2 : 1
			SMC				
N12.....	150	10^5	10×10^{17}	150	$(1–5) \times 10^2$	6×10^{17}	1 : 1
N27.....	30	10^5	0.6×10^{17}	60–100	10^2	0.6×10^{17}	1 : 1
N66.....	20–60	$10^4–10^5$	6×10^{17}	300	10^4	0.3×10^{17}	1 : 9
N83.....	10–30	10^4	$(1–2) \times 10^{17}$	100	3×10^3	0.3×10^{17}	1 : 8

whereas the parameters of the other are generally less tightly constrained.

4. SUMMARY AND CONCLUSIONS

A general result of our survey is the detection of significant ^{12}CO $J = 4 \rightarrow 3$ emission in most molecular peaks in the Magellanic Clouds. By itself this demonstrates the widespread occurrence of significant amounts of warm molecular gas, as tentatively suggested by Israel et al. (2003). Application of LVG model calculations show that molecular gas kinetic temperatures as high as $T_{kin} = 100–300$ K frequently occur. Detailed analysis of the objects for which multiple line ratios are available strongly suggests that the higher temperatures occur in cloud regions that are not very dense ($n_{H_2} = 10^2–10^3$ cm^{-3}) and that this gas is generally associated with colder (typically $T_{kin} = 10–60$ K) but much denser ($n_{H_2} = 10^4–10^5$ cm^{-3}) molecular gas. The simplified analysis possible in cases where fewer line ratios are available strongly suggests that the situation in those objects is similar. We note that recently reported observations of the N44 complex in the LMC by Kim et al. (2004) also show the presence of strong ^{12}CO $J = 4 \rightarrow 3$ emission, leading the authors to conclude the likely presence of very high densities ($n_{H_2} \approx 10^5$ cm^{-3}).

A few clouds are notable in our survey. Already mentioned is the case of SMCB1#1, a quiescent, compact molecular cloud devoid of any star-forming activity. It appears to be essentially homogeneous and of modest density ($n_{H_2} = 700$ cm^{-3}) but is surprisingly warm ($T_{kin} = 50$ K). As there are no known embedded heating sources, this temperature must be maintained by the environment of the cloud, located in the southwest region of the SMC Bar. The other two notable objects also occur in the SMC. N12 is likewise located in the southern part of the Bar. Here, both the dense and relatively tenuous molecular phases appear to be surprisingly hot ($T_{kin} = 150$ K). In N66, a very hot ($T_{kin} = 300$ K) and a cooler ($T_{kin} = 40 \pm 20$ K) phase coexist, *both* at a rather high density of the order of $n_{H_2} = 10^4$ cm^{-3}. This particular molecular cloud is a relatively small remnant in a large and luminous star-forming complex (see Rubio et al. 1996). It is almost certainly in an advanced stage of destructive processing; high densities and temperatures are consistent with such a situation (Rubio et al. 2000; Contursi et al. 2000).

Have we found signs of metallicity effects on the temperature equilibrium of the ISM in metal-poor environments? Given the measurement uncertainties and the dearth of comparable data sets on "normal" clouds in our own Galaxy, such findings cannot be asserted on the present measurements. It is suggestive, however, that high temperatures seem pervasive even in largely quiescent clouds such as SMCB1#1. This result should be taken with caution, as we suffer from a strong sample selection bias: the brightness of the optically thick ^{12}CO $J = 1 \rightarrow 0$ transition is proportional to the source temperature and beam filling fraction, and we have pointed toward the brightest ^{12}CO $J = 1 \rightarrow 0$ clouds. Thus, it may not be surprising that our clouds are warm. Furthermore, studies of Galactic photodissociation regions (e.g., S140: Draine & Bertoldi 1999; NGC 2023: Draine & Bertoldi 2000) find that H_2 in star-forming clouds is frequently warmer than the theoretical expectation. Similarly, the intensities of the mid-J CO lines tend to be underpredicted by homogeneous photodissociation region calculations (Hollenbach & Tielens 1999 and references therein). It is unclear whether these discrepancies are due to the presence of other heating mechanisms or to shortcomings in the models (e.g., Draine & Bertoldi 1999).

From the observational standpoint, a conclusive study of the effects of metallicity on gas temperature in the Magellanic Clouds must await the availability of more powerful submillimeter instruments observing the southern sky such as the Atacama Large Millimeter Array (ALMA) and the recently deployed single-dish telescopes: the Atacama Pathfinder Experiment (APEX) and the Atacama Submillimeter Telescope Experiment (ASTE).

We wish to thank the AST/RO group and the anonymous referee. A. D. B. wishes to thank D. Hollenbach for discussions on the subject of warm molecular gas and for suggestions that helped improve this manuscript. A. D. B. and C. L. M. acknowledge support from National Science Foundation grants AST 02-28963 and OPP-0126090, respectively.

REFERENCES

Bolatto, A. D., Jackson, J. M., Israel, F. P., Zhang, X., & Kim, S. 2000, ApJ, 545, 234
Bolatto, A. D., Leroy, A., Israel, F. P., & Jackson, J. M. 2003, ApJ, 595, 167
Chin, Y.-N., Henkel, C., Millar, T. J., Whiteoak, J. B., & Marx-Zimmer, M. 1998, A&A, 330, 901
Contursi, A., et al. 2000, A&A, 362, 310
Draine, B. T., & Bertoldi, F. 1999, in The Universe as Seen by *ISO*, ed. P. Cox & M. F. Kessler (ESA SP-427; Noordwijk: ESA), 553
———. 2000, in Molecular Hydrogen in Space, ed. F. Combes & G. Pineau de Forêts (Cambridge: Cambridge Univ. Press), 131
Garay, G., Johansson, L. E. B., Nyman, L.-Å., Booth, R. S., Israel, F. P., Kutner, M. L., Lequeux, J., & Rubio, M. 2002, A&A, 389, 977
Heikkilä, A. 1998, Ph.D. thesis, Chalmers Univ.
Heikkilä, A., Johansson, L. E. B., & Olofsson, H. 1999, A&A, 344, 817
Henize, H. 1956, ApJS, 2, 315
Hollenbach, D., & Tielens, A. G. G. M. 1999, Rev. Mod. Phys., 71, 173
Honingh, C. E., Delange, G., Dierichs, M. M. T. M., Schaeffer, H. H. A., Wezelman, J., Vandekuur, J., Degraauw, T., & Klapwijk, T. M. 1992, in Proc. 3rd Int. Symp. on Space Terahertz Technology, ed. F. T. Ulaby & C. A. Kukkonen (Washington: NASA), 251
Israel, F. P., de Graauw, Th., van de Stadt, H., & de Vries, C. P. 1986, ApJ, 303, 186
Israel, F. P., Tacconi, L. J., & Baas, F. 1995, A&A, 295, 599
Israel, F. P., et al. 1993, A&A, 276, 25
———. 2003, A&A, 406, 817
Jansen, D. J. 1995, Ph.D. thesis, Univ. Leiden
Jansen, D. J., van Dishoeck, E. F., & Black, J. H. 1994, A&A, 282, 605
Johansson, L. E. B., Olofsson, H., Hjalmarson, A., Gredel, R., & Black, J. 1994, A&A, 291, 89
Johansson, L. E. B., et al. 1998, A&A, 331, 857
Kim, S., Walsh, W., & Xiao, K. 2004, ApJ, 616, 865
Le Bourlot, J., Pineau Des Forêts, G., Roueff, E., & Flower, D. R. 1993, A&A, 267, 233
Leroy, A., Bolatto, A. D., Simon, J., & Blitz, L. 2005, ApJ, 625, 763
Lisenfeld, U., & Ferrara, A. 1998, ApJ, 496, 145
Madden, S. 2000, NewA Rev., 44, 249
Reach, W. T., Boulanger, F., Contursi, A., & Lequeux, J. 2000, A&A, 361, 895
Rubio, M., Boulanger, F., Rantakyro, F., & Contursi, A. 2004, A&A, 425, L1
Rubio, M., Contursi, A., Lequeux, J., Probst, R., Barbá, R., Boulanger, F., Cesarsky, D., & Maoli, R. 2000, A&A, 359, 1139
Rubio, M., et al. 1993, A&A, 271, 1
———. 1996, A&AS, 118, 263
Schieder, R., Tolls, V., & Winnewisser, G. 1989, Exp. Astron., 1, 101
Stark, A. A., et al. 2001, PASP, 113, 567
Taylor, C. L., Kobulnicky, H. A., & Skillman, E. D. 1998, AJ, 116, 2746
Walker, C. K., Kooi, J. W., Chant, M., Leduc, H. G., Schaffer, P. L., Carlstrom, J. E., & Phillips, T. G. 1992, Int. J. Infrared Millimeter Waves, 13, 785
Wolfire, M. G., Hollenbach, D., McKee, C. F., Tielens, A. G. G. M., & Bakes, E. L. O. 1995, ApJ, 443, 152